Precession driven low-latitude hydrological cycle paced by shifting perihelion

Hu Yang[1], Xiaoxu Shi[1], Xulong Wang[2], Qingsong Liu[3], Yi Zhong[3], Xiaodong Liu[2], Youbin Sun[2], Yanjun Cai[4], Fei Liu[5], Gerrit Lohmann[6], Martin Werner[6], Zhimin Jian[7], Tainã M. L. Pinho[6], Hai Cheng[4], Lijuan Lu[5,1], Jiping Liu[5,1], Chao-Yuan Yang[1], Qinghua Yang[5,1], Yongyun Hu[8], Xing Cheng[9], Jingyu Zhang[3], and Dake Chen[1]

[1]Southern Marine Science and Engineering Guangdong Laboratory, Zhuhai, China
[2]State Key Laboratory of Loess and Quaternary Geology, Institute of Earth Environment, Chinese Academy of Sciences, Xi'an, China
[3]Centre for Marine Magnetism, Department of Ocean Science and Engineering, Southern University of Science and Technology, Shenzhen, China
[4]Institute of Global Environmental Change, Xi'an Jiaotong University, Xi'an, China
[5]School of Atmospheric Sciences, Sun Yat-sen University, Zhuhai, China
[6]Alfred Wegener Institute, Helmholtz Centre for Polar and Marine Research, Bremerhaven, Germany
[7]Laboratory of Marine Geology, Tongji University, Shanghai, China
[8]Department of Atmospheric and Oceanic Sciences, School of Physics, Peking University, Beijing, China
[9]ShanXi Experimental Center of Geological Survey, ShanXi Institute of Geological Survey, Xi'an, China

Correspondence: Hu Yang (yanghu@sml-zhuhai.cn)

Abstract. Paleoclimate proxies reveal a significant precessional impact on the low-latitude hydrological cycle. Classical theory suggests that precession modulates the inter-hemisphere summer insolation difference, and hence controls the meridional displacement of the Inter-Tropical Convergence Zone. Accordingly, low-latitude precipitation variations are expected to be in-phase (for the Northern Hemisphere) or anti-phase (for the Southern Hemisphere) with the Northern Hemisphere summer

5   insolation. However, increasing number of proxies, particularly those absolutely dated ones, reveal that variations in terrestrial precipitation at different low-latitudes follow distinct precession rhythms that are very often out-of-phase with hemispheric summer insolation. The mechanism underlying such spatial complexity remains elusive. In this study, we argued that the precession driven low-latitude hydrological cycle is paced by shifting perihelion, rather than the hemispheric summer insolation. More specifically, precession of the Earth's rotation axis alters the occurrence season and latitude of perihelion. When perihe-

10   lion occurs, increasing insolation raises the moist static energy over land faster than over ocean due to differing thermal inertia. This thermodynamically moves the tropical convergence precipitation from the ocean to the land, contributing to enhancing the terrestrial precipitation over the latitudinal rain belt. As perihelion shifts towards different latitudes and seasons at different precessional phases, this leads asynchronous terrestrial precipitation maxima at different latitudes. Our hypothesis, supported by both model simulations and geologic records, suggests that the insolation in individual seasons is equally important in

15   shaping the orbital scale climate changes at low-latitude. This offers an alternative dynamical interpretation for the complex evolution of low-latitude hydrological cycle under precessional forcing.

1 Introduction

By redistributing solar radiation across different latitudes and seasons, Earth's orbital changes exerted a significant impact on past climate change (Milankovitch, 1941; Berger, 1978, 1988). In high-latitude regions, these orbital-scale climate changes
20 are characterised by cyclic expansion and retreat of ice sheets, with periodicities of ∼41 or ∼100 kilo-years (ka) (Lisiecki and Raymo, 2005), modulated by the Milankovitch cycles of obliquity and eccentricity (Milankovitch, 1941). In contrast, low-latitude climate changes are marked by periodic variations in hydrological cycle with dominant period of ∼23 ka, aligning with the Milankovitch cycles of precession (Clement et al., 2004; Cruz Jr et al., 2005; Braconnot et al., 2008; Carolin et al., 2013; Cheng et al., 2016; Wang et al., 2014a; Cheng et al., 2022). These precessional fluctuations are widely documented in
25 precipitation-related proxies from Asia, South America, and Africa (Kutzbach, 1981; Kuper and Kropelin, 2006; An et al., 2000; Cruz Jr et al., 2005; Wang et al., 2007, 2008; Carolin et al., 2013, 2016; Li et al., 2024). Among these changes, the periodic greening of the Sahara stands out as one of the most fascinating phenomena (Kutzbach, 1981; Kuper and Kropelin, 2006; DeMenocal et al., 2012; Armstrong et al., 2023).

Low-latitudes precipitation primarily comes from the seasonal migration of the Inter-Tropical Convergence Zone (ITCZ,
30 Fig. 1a) (Gadgil, 2018). Early studies proposed that precession regulates the inter-hemispheric summer insolation difference and modulates the meridional migration of the ITCZ (Kutzbach, 1981; Wang et al., 2014a; Schneider et al., 2014). Increased summer insolation in the Northern Hemisphere (perihelion) corresponds to decreased summer insolation in the Southern Hemisphere (aphelion). Accordingly, variations in terrestrial precipitation are expected to align with changes in summer insolation, exhibiting an anti-phase relationship between the Northern and Southern Hemispheres (Wang et al., 2004; Cruz Jr et al., 2005;
35 Cheng et al., 2013; Wang et al., 2014a, 2017) (Fig. 1b and 1d). However, in the past two decades, an increasing number of proxies have shown that although low-latitude terrestrial precipitation displays significant precessional variations, their evolution patterns are not necessarily in-phase with the Northern/Southern Hemisphere summer insolation (An et al., 2000; Clemens and Prell, 2007; Carolin et al., 2013, 2016; Zhou et al., 2022). For example, the reconstructed onsets and optimums of the East Asian summer monsoon at different geographical locations were asynchronous with the Northern Hemisphere summer insola-
40 tion (An et al., 2000; Cai et al., 2010; Ran and Feng, 2013; Chen et al., 2015; Liu et al., 2015; Zhou et al., 2022). The Indian summer monsoon, reconstructed from sediment cores of the Arabian Sea, shows an early Holocene optimum (Thamban et al., 2007), significantly preceding that of the East Asian summer monsoon (Sun et al., 2006; Liu et al., 2015). Around the equator, a Malaysian speleothem record, reflecting local precipitation strength, exhibits an evolutionary pattern neither comparable to the Northern Hemisphere summer insolation nor the Southern Hemisphere summer insolation (Carolin et al., 2013) (Fig. 1c). Over
45 Africa, archaeological and geological evidence indicates that the recent termination of the greening Sahara occurred earlier in north Africa than in the south (Kuper and Kropelin, 2006; Shanahan et al., 2015).

The cause of the asynchronous relationship between terrestrial precipitation and summer insolation has been investigated extensively form both modelling and proxy-model comparison perspectives (Short and Mengel, 1986; Braconnot and Marti, 2003; Zhao et al., 2005; Kuper and Kropelin, 2006; Clemens and Prell, 2007; Shanahan et al., 2015; Ran and Feng, 2013; Chen
50 et al., 2015; Cheng et al., 2021; Zhou et al., 2022). These studies hypothesis that summer insolation's control on the low-latitude

hydrological cycle could be disrupted by a variety of factors, including internal ocean-atmosphere feedback (Clemens and Prell, 2007), present of ice sheet (Chen et al., 2015), development of vegetation (Cheng et al., 2021), delayed ocean warming (Ran and Feng, 2013) and sea level fluctuations (Griffiths et al., 2009). Interestingly, transient and time-slice simulations with solely insolation forcing also yield an asynchronous precipitation response to hemispheric summer insolation (Braconnot and Marti,

55   2003; Kutzbach et al., 2008; Erb et al., 2015; Liu et al., 2022). This raises question of whether terrestrial precipitation does not follow changes in hemispheric summer insolation. By performing simulations with different precessional phases, Braconnot and Marti (2003) found that the occurrence time of maximum insolation (perihelion) affect the seasonality of Indian monsoon. They proposed that insolation in other seasons may also important, especially in determining the seasonal timing of Indian summer monsoon. Focusing on the East Asian monsoon, Zhou et al. (2022) suggested that insolation in different months may

60   contribute to a time-transgressive pattern of East Asian monsoon optimum at different latitudes. By running an isotope-enabled transient simulation covering the past 300 ka, Liu et al. (2022) found that the precipitation $\delta^{18}O$ in Asia is primarily affected by the temperature and insolation during the rainy seasons, rather than the averaged boreal summer insolation.

    In this study, we performed theoretical analysis, climate simulations and geological records, to hypothesis that low-latitude hydrological cycle is paced by shifting perihelion, rather than the hemispheric summer insolation.

65   2   Methodology

2.1   Model Simulations

Using AWI- Earth System Model (AWI-ESM, (Sidorenko et al., 2015, 2019)), we perform two set of experiments to study the mechanism of precessional impact on low-latitude hydrological cycle. The AWI-ESM is a coupled ocean-atmosphere model. It consists of the atmospheric component ECHAM6 (Giorgetta et al., 2013) and the oceanic component FESOM (Wang et al.,

70   2014b; Danilov et al., 2017). The oceanic component employs an unstructured-mesh, with relatively high resolution (up to 25 km) at polar regions, coast areas and the equator, while the atmospheric component has a spatial resolution of 1.875°. Detailed information on the model setup can also be found in Shi et al. (2016) (Shi and Lohmann, 2016).

2.1.1   Idealised Earth system without tilted Earth rotation axis

In the first experiment, we create an idealised Earth system without seasonal migration of Sun's zenith point (obliquity=0),

75   while introducing a relatively elliptical orbit (eccentricity=0.058). In this experiment, perihelion takes place in June and aphelion takes place in December. We run the simulation for 1000 years, with the last 100 years result used for analysis. This experiment is designed aiming to test how changing Earth-Sun distance affects the tropical precipitation over land.

2.1.2   Simulations reconstructing a precessional cycle

In the second step, we perform another set of experiments to reconstruct the climate change within a precessional cycle. In these

80   simulations, the obliquity is set to be 24.5°. Twenty-four sensitivity simulations were performed using different precessional

phases, i.e., 0°, 15°, 30°, ... 345°. To allow the low-latitude climate to reach a quasi-equilibrium state to insolation forcing, we integrated the model for 300 years, and the last 100 years mean climate were used to represent the climate at the corresponding precession phase. This approach removes the natural climate variability, such as El Nino–Southern Oscillation.

All these 24 simulations are initialized from a pre-industrial simulation which had participated in the PMIP4 project. For all simulations, the greenhouse gas concentrations in the atmosphere, land-sea distribution and ice sheet configuration are fixed as the pre-industrial condition.

Natural climate variability is ubiquitous that sometimes conceals external forcing. To highlight the external precessional forcing in climate change, in all simulations, the eccentricity is set to a relatively high value (0.058). Consequently, this configuration exposes the Earth to 26% more solar radiation during perihelion than during aphelion. Additionally, we examine the climatology mean of the last 100 years model results. This further eliminates the contribution of natural variability on simulated climate changes.

Due to differences in the Earth's revolution speed, the length of four seasons varies depending on the precessional configurations. This leads the "calendar effect" (Joussaume and Braconnot, 1997; Shi et al., 2022) . In our results, we use the present day calendar, with the spring equinox set at March 21. As a results, the dates of the summer solstice, autumnal equinox, and winter solstice can be changed a couple of days depending on the precessional configurations. Since our analysis is based on monthly results, we do not make any additional corrections on these dates in order to keep consistency.

2.2 Speleothem Proxies

Speleothem $\delta^{18}O$ records from China (Cheng et al., 2016), Malaysia (Carolin et al., 2013, 2016) and Brazil (Cruz Jr et al., 2005) are used in this study. The record from China is composited by (Cheng et al., 2016) based on several records from Sanbao (31°40' N, 110° 26' E), Hulu (32° 30' N, 119° 10' E) and Dongge (25° 17' N, 108° 5' E) caves (Wang et al., 2001; Dykoski et al., 2005; Kelly et al., 2006; Wang et al., 2008; Cheng et al., 2009). The Malaysia records were collected in different caves in Gunung Mulu National Park, Borneo, Malaysia ((4°N, 115°E) (Carolin et al., 2013, 2016). The Brazil record is collected from the Botuvera Cave (27° 13' 24" S, 49° 09' 20" W) (Cruz Jr et al., 2005).

2.3 Method

The Empirical orthogonal functions (EOF) analysis is used to identify the spatial and temporal characteristics of terrestrial precipitation at low latitudes. EOF analysis is widely applied in Earth science. It is generally used to simplify a spatial-temporal data set by converting it into spatial patterns of variability and temporal evolution of these patterns. For the idealised Earth system experiment without tilted Earth rotation axis, we applied EOF analysis on the climatology monthly convective precipitation (Fig. 3). For the 24 simulations recovering a precessional cycle, we applied EOF analysis on the individual monthly convective precipitation. For example, December precipitation in the 24 simulations are selected and applied a EOF analysis to generate Fig. 4a.

The ITCZ precipitation takes place over the Earth warmest region, i.e., the thermal equator. To determine the geographical location of the thermal equator, we calculate the moist static energy (analogous to equivalent potential temperature) using the following equation:

115
$$S = C_p \cdot T + g \cdot z + L_v \cdot q \tag{1}$$

where S is the moist static energy, C_p is the specific heat at constant pressure, T is the absolute air temperature, g is the gravitational constant, z is the geopotential height above sea level, L_v is the latent heat of vaporization, and q is water vapor specific humidity (Neelin and Held, 1987; Wallace and Hobbs, 2006).

The latitude of the perihelion is introduced as the latitude of Sun's zenith point when perihelion occurs. This latitude also
120 represents the latitude of maximum incoming solar radiation at the top of atmosphere. The insolation characteristics are calculated using MATLAB with aids from two tools, namely the "Orbital, the Box" (Lougheed, 2021) and the Earth Orbit Model v2.1 (Kostadinov and Gilb, 2014). These tools were developed based on the theoretical framework presented in (Berger, 1978; Laskar, 1990; Laskar et al., 1993).

3   Precession shifts the season and latitude of perihelion

125 To understand the mechanism of how precession governs low-latitude hydrological cycle, we first look at how precession affects the solar radiation received by Earth.

The Earth's orbit around the Sun is not a perfect circle, but an ellipse. When the Earth's distance from the Sun is at its shortest, i.e., perihelion, it receives the strongest solar radiation. Currently, perihelion happens in boreal winter, when the Sun's zenith point closes to the Tropic of Capricorn. By changing the orientation of the Earth's rotation axis, precession gradually
130 delays the occurrence of perihelion by around 20.4 minutes per year. About 11 kiloyears ago, perihelion occurred in boreal summer, when the Sun's zenith point closest to the Tropic of Cancer (Hunt et al., 2023). Therefore, precession not only shifts the occurrence season of perihelion, but also the "latitude of perihelion". Here, the latitude of perihelion is introduced as the latitude of Sun's zenith point when perihelion occurs. Supplementary Movie 1 further clarify this.

To precisely describe when and where perihelion occurs, Fig. 2 details the season and latitude of perihelion at different
135 precessional phases (longitude of perihelion). Similar to the movement of the Sun's zenith point over the course of a year, the latitude of perihelion migrates between Tropics of Cancer and Capricorn over the course of a precessional cycle. Whenever (the season) and wherever (the latitude) perihelion occurs, the insolation in the corresponding season and the perihelion latitude reaches its maximum in a precessional cycle (Supplementary Movie 1). Maximum insolation (perihelion) potentially drives anomalous climate changes on Earth.

4 Perihelion promotes tropical convective precipitation over land

To investigate how perihelion impacts low-latitude climate change, we conducted an idealised Earth system experiment using AWI-ESM (Sidorenko et al., 2015, 2019). In this idealised Earth system, the Earth's rotation axis is not tilted (zero obliquity). The Earth's orbit is set to be relatively elliptical (see Model Simulations). As a result, the thermal equator and the associated tropical rain belt are constrained in the vicinity of geographic equator. However, due to variations in the distance between Earth and Sun, the temperature and precipitation exhibits a seasonality (Fig. 3).

When perihelion occurs, the incoming solar radiation maximises. Due to different thermal inertia between the land and the ocean, the atmospheric heating over land is much stronger than that over the ocean. This leads to faster increase in moist static energy over the land than the ocean (Fig. S2). As tropical convective precipitation tends to occur towards the warmest regions with highest moist static energy (Neelin and Held, 1987; Battisti et al., 2014; Schneider et al., 2014; Geen et al., 2020), we observed maximum convective precipitation over land (minimum convective precipitation over ocean) 1-2 month after the perihelion (Fig. 3 and S2). In brief, perihelion can promote tropical precipitation over land. With this understanding, we switch to a more complex Earth system with tilted Earth's rotation axis and shifting perihelion.

5 Seasonal terrestrial precipitation peaks whenever and wherever perihelion occurs

We conducted another set of numerical experiment using AWI-ESM. This time, the Earth's rotation axis is tilted (obliquity=24.5°). Therefore, the Sun's zenith point marches between the Tropics of Cancer and Capricorn, driving a seasonal migration of terrestrial precipitation (Fig. S3). We manipulated precessional phase to reconstruct the climate changes over the course of a precessional cycle (see Methodology). Specifically, 24 time-slice simulations were performed with the precessional phase (namely the longitude of the perihelion) varying from 0° to 345° with an interval of 15° (Fig. 2). Due to different precessional phases, when (the season) and where (the latitude) the perihelion takes place vary among these experiments (Fig. 2).

Since the low-latitude terrestrial precipitation is concentrated at different latitudes in different months, we examined for each individual month the precipitation evolution in a precessional cycle. Empirical Orthogonal Functions (EOF) analysis was applied to explore the spatial and temporal characteristics of terrestrial precipitation oscillation. This allows us to identify where (the latitudes) and when (the precessional phase) the terrestrial precipitation peaks.

In February, the ITCZ and predominant terrestrial precipitation locates at its southernmost latitudes (Fig. 4f, contours). We found the strongest February terrestrial precipitation around precessional phase of -75° (Fig. 4f, blue line). This corresponds to the perihelion occurring one month earlier (in January, as shown in Fig. 4f with a colored circle) at its southernmost latitudes.

The ITCZ and associated rain belt locates around the equator in April (Fig. 4e, contours). We found the strongest April precipitation around the precessional phase of 15° (Fig. 4e, blue line) when perihelion occurs in March, with the latitude of perihelion being around the equator (Fig. 4e, colored circle).

Following the seasonal migration of Sun's zenith point, the rain belt moves northward and reaches its northernmost position in August (Fig. 4c, contours). Within a precession cycle, August terrestrial precipitation peaks near precessional phase of 120°

(Fig. 4c, blue line), corresponding to a late July perihelion. This means that the perihelion is almost at its northernmost latitudes (Fig. 4c, colored circle).

From August to February, the terrestrial precipitation migrates southward, completing an annual cycle. Whenever (the season) and wherever (the latitude) perihelion occurs, the related seasonal and latitudinal terrestrial precipitation reaches its maximum. This leads asynchronous terrestrial precipitation maxima at different seasons and latitudes (Fig. 4, blue arrow).

There is good co-variation between the seasonal insolation intensity (Fig. 4, black lines), land surface temperature (Fig. 4, red lines) and terrestrial precipitation (Fig. 4, blue lines). We propose that perihelion maximises the incoming solar radiation and drives the greatest land-sea heating contrast. This thermodynamically moves the tropical convergence zone from ocean to land (Fig. S4) (Battisti et al., 2014), and forces the strongest seasonal terrestrial precipitation within a precessional cycle. Due to the thermal inertia of the Earth, the thermal equator and seasonal terrestrial precipitation do not synchronise with the insolation in the same month, but rather the insolation at approximately 1-2 month earlier. In agreement, such a delay has been also revealed by many other model simulations (Kutzbach et al., 2008; Erb et al., 2015; Donohoe et al., 2020; Liu et al., 2022).

Moving perihelion introduces strongest solar radiation across different seasons and latitudes, and forces strongest terrestrial precipitation in the corresponding season and latitudes (Fig. 5). Theoretically, for the tropical area between the Tropics of Cancer and Capricorn, there are two occurrences of perihelion within a precession cycle. For instance, at the equator, the first perihelion occurs at precessional phase of 0° around the spring equinox (Fig. 2). The second perihelion occurs at precessional phase of 180° around the autumnal equinox (Fig. 2). Consequently, at the equator, the temporal interval between these two perihelion events spans half of a precessional cycle, resulting in cyclic variations in precipitation with a period of half of a precession cycle (Fig. 5c).

For the area outside the equatorial zone, the time interval between the two successive perihelion events varies across different latitudes (Fig. 2 and Supplementary Movie 1). With increasing latitude, these two perihelion events take place closer to each other, and merge into a single insolation and precipitation maximum at latitudes higher than the Tropic of Cancer (Fig. 2). This phenomenon is evident in our analysis of monthly precipitation patterns derived from zonal mean precipitation in different latitudinal belts (Fig. 5).

6 Evidence from geologic records

Besides model simulations, a realistic precession cycle can also be examined in the sparse-distributed geologic archives. There is a relatively abundant collection of proxies for the most recent precession cycle, spanning the past 23 ka. However, these records may not be ideal for deriving precession-associated climate changes, due to the limitation of the relatively low eccentricity (Berger, 1978, 1988), which diminishes the influence of precession on driving climate variations (Fig. S5) (Braconnot and Marti, 2003; Bosmans et al., 2018; Chiang et al., 2022; Beaufort and Sarr, 2023; Wu et al., 2023). Moreover, the scenario becomes more complex due to a variety of factors, such as the rapid disintegration of ice sheets, rising sea level, increasing greenhouse gas concentrations, and abrupt climate changes (Griffiths et al., 2009; Weber and Tuenter, 2011; Wang et al., 2014a; Chen et al., 2015; Chiang and Friedman, 2012; Clemens et al., 2021). Given the amplification of the precessional signal during

7

205 periods of high eccentricity (Chiang and Broccoli, 2023) (Fig. S5), our investigation focused on the interval spanning 66-133 ka, thus encompassing three complete precessional cycles.

Many proxies' chronology is astronomically tuned to the Northern Hemisphere summer insolation, making them inappropriate to address the asynchronous signals at different latitudes. Here, we utilize the absolute-dated speleothem $\delta^{18}O$ records which were widely used as proxies of precipitation amount, despite the facts that they are somewhat also affected by precipi-

210 tation source $\delta^{18}O$ and temperature (Cruz Jr et al., 2005; Lachniet, 2009; Cai et al., 2010). We synthesize proxies from China (Cheng et al., 2016), Malaysia (Carolin et al., 2013, 2016) and Brazil (Cruz Jr et al., 2005) to validate our hypothesis (Fig. 1). These records are selected because they are representative of three typical regions (i.e., northern limit, equator and southern limit of low-latitude) and have continuous long coverage and high-resolution Uranium-Thorium chronologies. Moreover, these records also well document the precessional dominated precipitation variations.

215 Speleothem records are seasonally-biased towards their growing seasons, which are usually the rainy seasons (Kwiecien et al., 2022; Liu et al., 2022). Modern observations indicate that the rainy season near the Chinese proxies is boreal summer, whereas the dominant rainy season in Brazil is boreal winter. In the vicinity of Malaysia, there are two prevailing rainy seasons, namely the boreal spring and autumn (Fig. S1). Accordingly, we expect that the $\delta^{18}O$ signals in the selected regions reflect precipitation changes in their corresponding seasons.

220 As depicted in Fig. 1b, the latitude of perihelion reaches its northernmost position at 90° precessional phase (Fig. 1b, dashed line, and Fig. 2 and S2b), corresponding to maximum insolation in boreal summer and maximum in Eastern Asian summer precipitation. Around the precessional phase of 180°, the latitude of perihelion is close to the equator, corresponding to maximum insolation in autumnal equinox (Fig. 2 and S2c). The maximum boreal autumn insolation drives the maximum equatorial precipitation, as evidenced by the speleothem record from Malaysia (Fig. 1c). When perihelion migrates to its

225 southernmost position, i.e., at precessional phase 270° (Fig. 2 and S2d), the precipitation optimum is identified in Brazil, in agreement with the boreal winter insolation maxima (Fig. 1d). At a precessional phase of 0°, perihelion occurs around the equator in spring equinox (Fig. 2 and S2a). This leads to maximal insolation in March (Fig. 1c, grey line). We find maximum precipitation signals in the Malaysia speleothem record (Fig. 1c, red line) around 110.9 and 88.5 ka, corresponding to two maxima in March insolation. The perihelion moves to its northernmost position at precessional phase of 90°, thus completing a

230 full precessional cycle. We noticed that the manifestation of October insolation in the half precessional signals in the Malaysia record is relatively stronger than that of the insolation in March. This is likely attributed to a stronger boreal autumn rain than the boreal spring rain (Fig. S1).

The results based on the speleothem records again suggest that wherever the perihelion occurs, the local terrestrial precipitation peaks. This exhibits an asynchronous precipitation maxima following the meridional migration of perihelion (Fig. 1,

235 dashed line). Near the equator, half-precessional signals are identified, in agreement with our model simulations (Fig. 5) and many other records from the tropical area (Trauth and Strecker, 1996; Trauth et al., 2003; Verschuren et al., 2009; Jian et al., 2020).

It is interesting to note that shifting perihelion causes changes in the rainy seasons. Earlier study found that the shift of maximum summer insolation have strong impact on the Asian monsoon (Braconnot and Marti, 2003). Boreal spring perihelion

240 leads early northward migration of Northern Hemisphere westerly jet (Wu et al., 2023). In our simulations, we identified that the rainy season can shift from June to September near the 10°N latitudinal belt. At the equator, the dominant rainy season switches from April to October following the shift in perihelion (Fig. 5). This could complicate the comparison between proxies and models, as variations in the rainy seasons cannot be distinguished by proxies (Kwiecien et al., 2022).

7   Discussions and Conclusion

245 Many transient simulations have been conducted to investigate the dynamics of orbital-scale climate changes. These simulations introduced transient forcing attributed to changing Earth's orbit (Kutzbach et al., 2008; He, 2011; Liu et al., 2022), CO_2, land-sea mask and ice-sheet configurations (Liu et al., 2009). Despite been more realistic, the simulations with various forcing factors have added difficulty to disentangle the dynamics of precession's impact on low-latitude climate changes (Chen et al., 2015; Cheng et al., 2021; Griffiths et al., 2009; Ran and Feng, 2013). Time-slice simulations with precession extremes were
250 also performed (Kutzbach, 1981; Braconnot et al., 2008; Battisti et al., 2014; Erb et al., 2015; Bosmans et al., 2018; Jalihal et al., 2019) to assess the precession's role in climate change. However, they are unable to capture the diverse evolution patterns of low-latitude precipitation, as revealed by proxies (An et al., 2000; Wang et al., 2004; Cruz Jr et al., 2005; Cheng et al., 2013; Carolin et al., 2013, 2016; Zhou et al., 2022). In this study, we performed simulations purely forced by varying precessional phase. The results reveal that the low-latitude terrestrial precipitation maxima follows a shifting perihelion, with a time lag of
255 1-2 months.

Traditionally, low-latitude precipitation was regarded as a manifestation of global monsoon, which usually defined as occurring in hemispheric summer (Wang and Ding, 2008; Wang et al., 2014a, 2017; Geen et al., 2020). Therefore, inter-hemispheric summer insolation difference was considered as the main driver of precipitation changes at low-latitudes (Wang et al., 2014a; Schneider et al., 2014). Under this framework, the non-summer precipitation has received less attention. In reality, the ITCZ
260 related precipitation occurs in different seasons (Fig. S3), not necessary during the hemispheric summer. Therefore, a comprehensive hypothesis should explain precipitation changes not only in the hemispheric summer, but also that in other seasons. We find that shifting perihelion likely plays a more important role in the fluctuations of seasonal and latitudinal tropical precipitation.

Several studies have shown that the distance effect, or perihelion and aphelion, has an impact on low-latitude seasonality in
265 addition to the Sun's zenith point march (Braconnot et al., 2008; Chiang et al., 2022; Beaufort and Sarr, 2023; Wu et al., 2023; Chiang and Broccoli, 2023; Hunt et al., 2023). Increased solar radiation can thermodynamically shift the tropical convergence zone from ocean to land (Battisti et al., 2014), thus the terrestrial precipitation is enhanced when perihelion occurs. Perihelion occurs in different seasons and latitudes, driving enhancement of terrestrial precipitation in the corresponding seasons and latitudes. From this point of view, insolation in individual season is equally important in determining the evolution of low-
270 latitude precipitation.

Astronomical tuning is widely used to establish the chronology of paleo proxies. By doing this, the phasing of proxies is artificially synchronized. However, our results indicate that the astronomically driven climate changes can naturally follow diverse rhythms. This questions the reliability of astronomical tuning strategy, at least for the low-latitudes area.

We interpreted how precession affects the low-latitude hydrological cycle. Meanwhile, sensitivity simulations indicate that

275   changing obliquity, greenhouse gas concentrations, ice sheets (Weber and Tuenter, 2011; Wang et al., 2014a; Chen et al., 2015; Chiang and Friedman, 2012; Clemens et al., 2021; Erb et al., 2015; Bosmans et al., 2018; Lyu et al., 2021) and millennial-scale Dansgaard-Oeschger events (Chiang and Friedman, 2012) all affect the ITCZ and low-latitude precipitation. For example, increased obliquity enhances the hemispheric summer insolation, therefore, contribute to increasing the terrestrial precipitation in the hemispheric summer (Erb et al., 2015; Bosmans et al., 2018). The combination of different forcings can lead a complex

280   evolution of precipitation changes, as recorded in proxies (Carolin et al., 2013; Yuan et al., 2023).

By detailing the position and seasonal timing of perihelion (Fig. 2), the precession-induced terrestrial precipitation maxima can be easily predicted at a given latitude and season. Currently, perihelion takes place around the Tropic of Capricorn, the southern hemisphere summer monsoon is relatively strong. Over the next few thousand years, following the movement of perihelion towards the equator, the equatorial terrestrial precipitation around the spring equinox will be enhanced. Compared

285   to the classical theory which highlights the role of summer insolation, our hypothesis provides a more comprehensive and plausible explanation for the asynchronous pattern of low-latitude precipitation variations raised from precessional forcing.
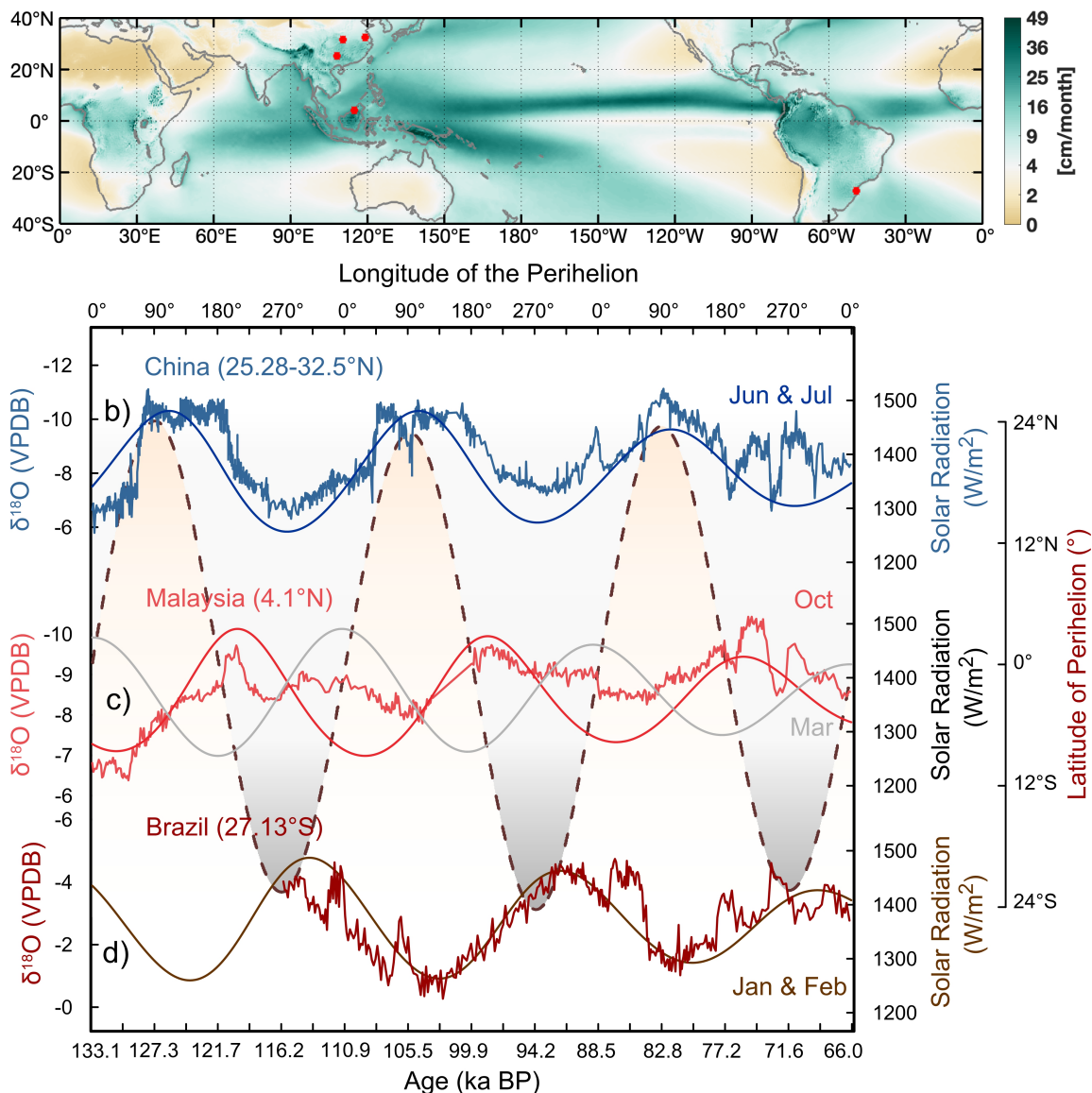
Figure 1. (a) Climatology map of annual mean precipitation over low-latitudes. Stalagmite oxygen isotope evolution in (b) China (Cheng et al., 2016) (c) Malaysia (4.1°N, 114.9°E) (Carolin et al., 2013, 2016) and (d) Brazil (27°13' 24" S, 49°09' 20" W) (Cruz Jr et al., 2005). The locations of these records are shown in Fig. 1a. The intensity of solar radiation in the rainy seasons are plotted as well: for China, it is the averaged solar radiation in June and July; for Malaysia, it is the solar radiation in October and March; for Brazil, it is the mean solar radiation in January and February. The dashed line illustrates the latitude of perihelion (see detailed definition in section 2). To better illustrate the terrestrial precipitation optimums at different precessional phases, we translate the age into precessional phase, which is shown in the upper axis. When the perihelion passes certain latitude, the seasonal solar radiation and terrestrial precipitation reach their maxima.
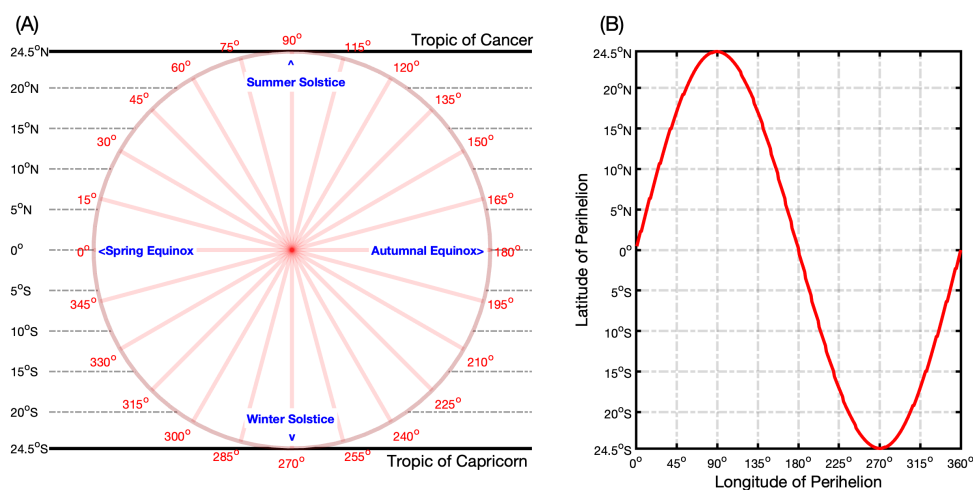
Figure 2. The latitudinal movement of the perihelion and Sun's zenith point within a precessional cycle and an annual cycle, respectively. The labels outside the circle give the precessional phase, namely the longitude of the perihelion. The labels inside the circle locate the position of season. Within a year, the Sun's zenith point march between the Tropic of Cancer and the Tropic of Capricorn. Within a precessional cycle, the latitude of perihelion also migrates between the Tropic of Cancer and the Tropic of Capricorn. The grey dashed lines give the latitudinal coordinate. When the perihelion occurs, the insolation at the perihelion latitude reaches the maximum within a precessional cycle. To better understand this figure, please also check Supplementary Movie 1 (https://zenodo.org/doi/10.5281/zenodo.11395458), which visually conveys an explanatory description of the seasonal solar radiation variations within a precessional cycle.
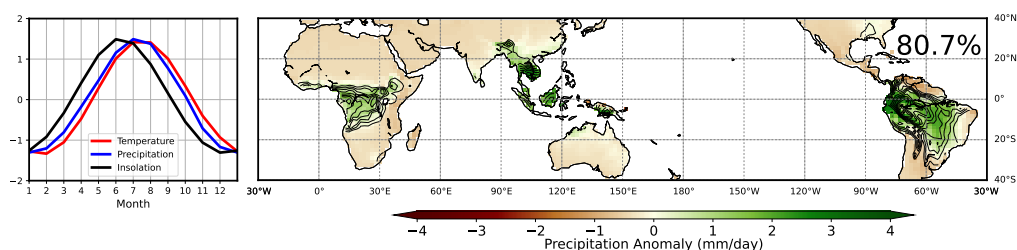
Figure 3. Temporal and spatial evolutions of terrestrial precipitation in the idealised Earth system experiment, with zero obliquity and high eccentricity (0.058). The shading color in the right panel illustrates the spatial pattern of the leading mode (contains 80.7% of terrestrial precipitation covariance) of Empirical Orthogonal Function (EOF) analysis on the monthly convective precipitation over land. The contours illustrate the climatology precipitation. The blue lines in the left panels show the corresponding principal component, illustrating the temporal evolution of the terrestrial precipitation strength. The area-weighted land-surface temperature (red line) and incoming solar radiation (black line) evolution are plotted as well. In this experiment, perihelion occurs in June, corresponding to maximum incoming solar radiation in June and maximum precipitation over land 1-2 month later (July and August).
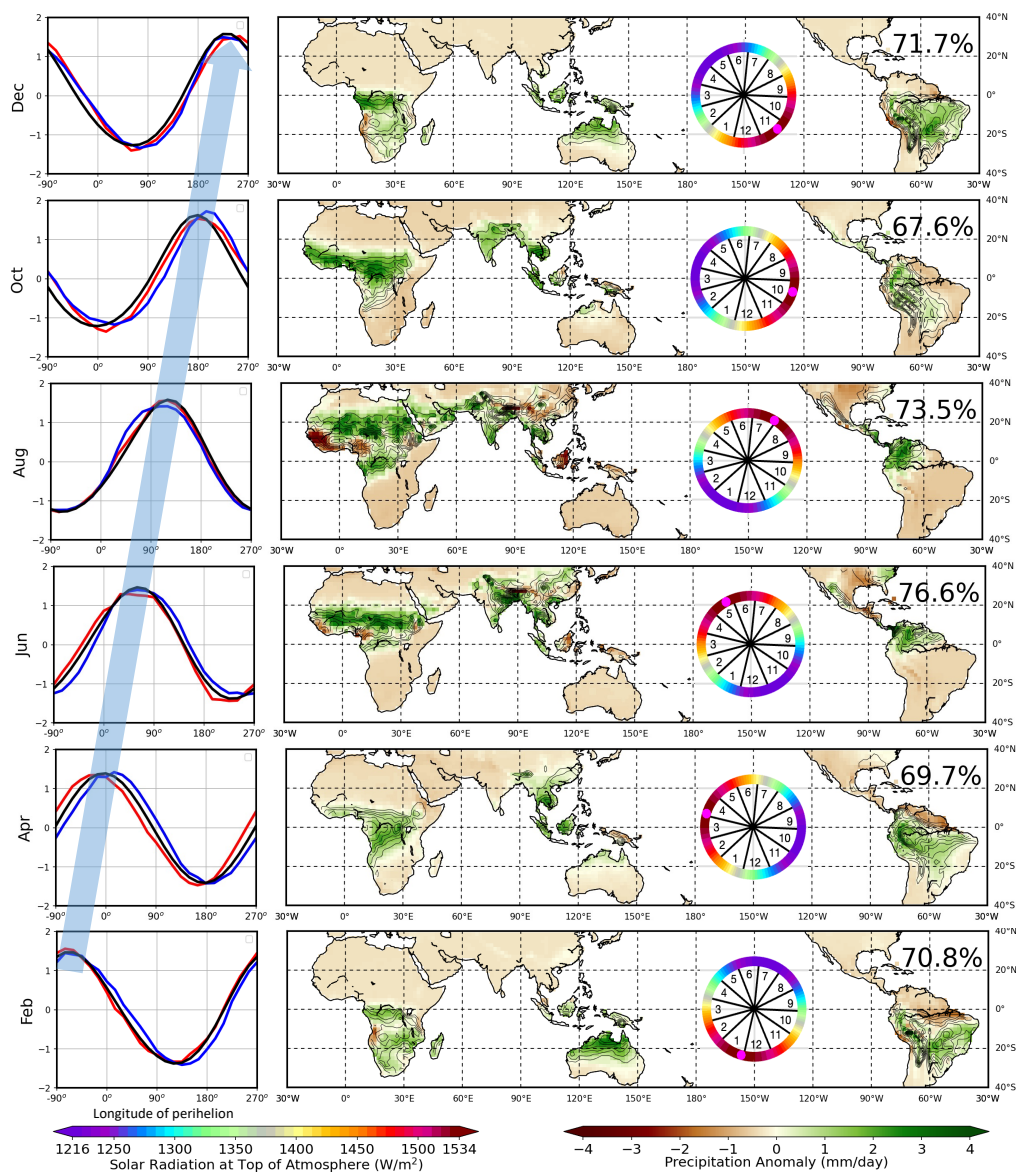
Figure 4. Temporal and spatial evolutions of terrestrial precipitation in different seasons. The shading color in the right panel illustrates the spatial pattern of the leading mode of Empirical Orthogonal Function (EOF) analysis on the monthly terrestrial precipitation simulated by AWI-ESM recovering a precessional cycle. The numbers in the subpanels' upper-right corner displays the contribution of the first principal component of EOF to the overall variance. The contours illustrate the climatology precipitation. The blue lines in the left panels show the corresponding principal component, illustrating the temporal evolution of the terrestrial precipitation strength. The area-weighted land-surface temperature (red line) and incoming solar radiation (black line) evolution are plotted as well. Note that, the plotted solar radiation is from an earlier month. For example, for the panel of February, the solar radiation in January is plotted. For comparison, all time-series are normalised. The colored circles illustrate the solar radiation distribution when the corresponding seasonal terrestrial precipitation peaks. The numbers in this circle give the location of the individual month. The pink dots give the timing and meridional position of perihelion. The blue patches illustrate the approximate location of the thermal equator and rain belt on land.
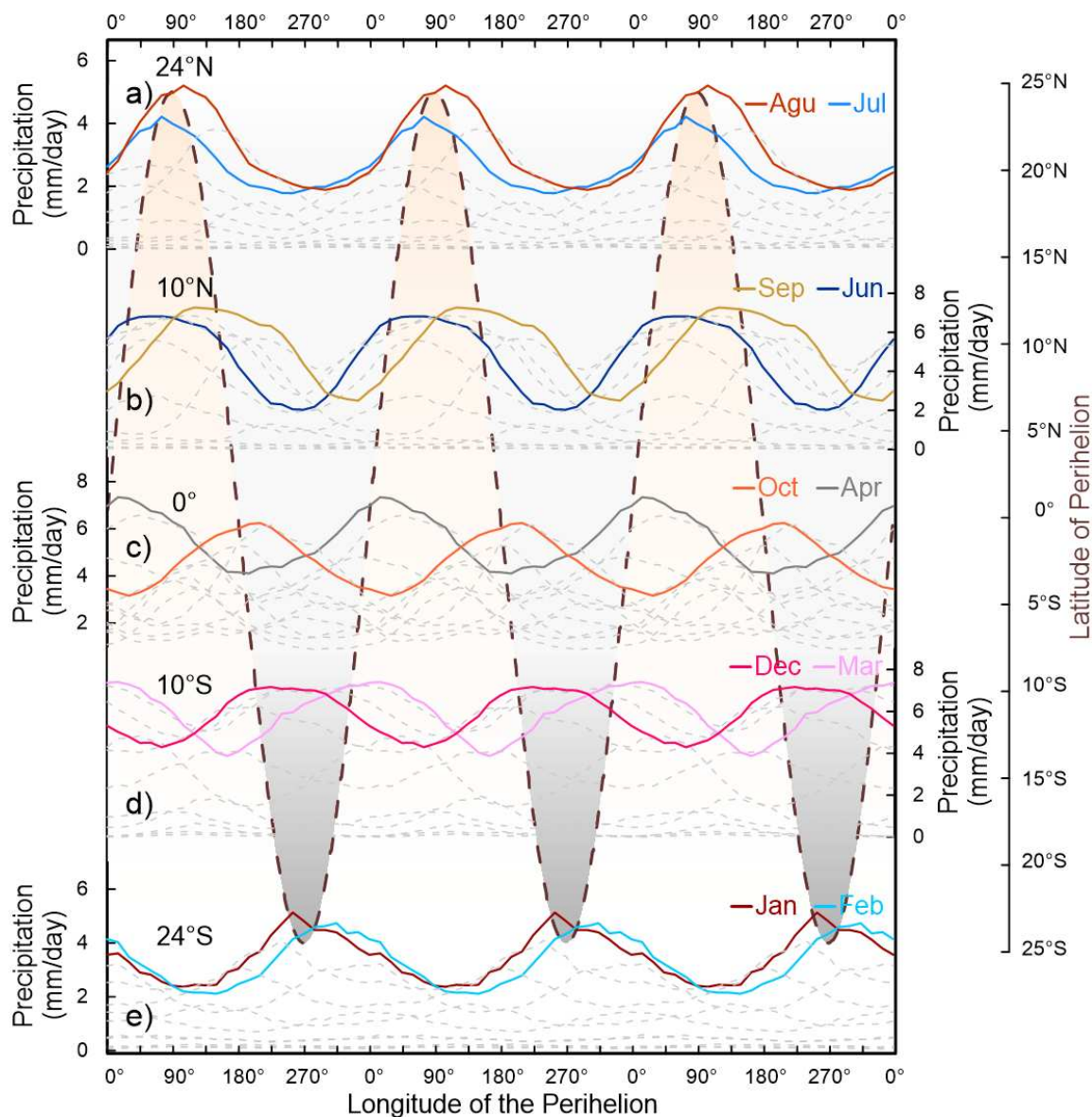
Figure 5. The simulated evolution of monthly precipitation at different latitudinal bands over three precessional cycles. The precipitation is calculated as zonal mean terrestrial precipitation over latitudinal bands covering a width of five degrees. For each latitudinal band, the rainy seasons are highlighted with colored lines, and precipitation in other months is shown as grey dashed lines. The dashed copper line illustrates the meridional movement of Earth's perihelion between the Tropic of Cancer and the Tropic of Capricorn, namely the latitude of perihelion. Whenever (the season) and wherever (the latitude) perihelion occurs, the local terrestrial precipitation in the corresponding month reaches its maximum within a precessional cycle.

References

295 An, Z., Porter, S. C., Kutzbach, J. E., Xihao, W., Suming, W., Xiaodong, L., Xiaoqiang, L., and Weijian, Z.: Asynchronous Holocene optimum of the East Asian monsoon, Quaternary Science Reviews, 19, 743–762, 2000.

Armstrong, E., Tallavaara, M., Hopcroft, P. O., and Valdes, P. J.: North African humid periods over the past 800,000 years, Nature Communications, 14, 5549, 2023.

Battisti, D., Ding, Q., and Roe, G.: Coherent pan-Asian climatic and isotopic response to orbital forcing of tropical insolation, Journal of
300   Geophysical Research: Atmospheres, 119, 11–997, 2014.

Beaufort, L. and Sarr, A. C.: Eccentricity forcing on Tropical Ocean Seasonality, Climate of the Past Discussions, 2023, 1–32, 2023.

Berger, A.: Long-term variations of daily insolation and Quaternary climatic changes, Journal of Atmospheric Sciences, 35, 2362–2367, 1978.

Berger, A.: Milankovitch theory and climate, Reviews of geophysics, 26, 624–657, 1988.

305 Bosmans, J., Erb, M., Dolan, A., Drijfhout, S., Tuenter, E., Hilgen, F., Edge, D., Pope, J. O., and Lourens, L.: Response of the Asian summer monsoons to idealized precession and obliquity forcing in a set of GCMs, Quaternary Science Reviews, 188, 121–135, 2018.

Braconnot, P. and Marti, O.: Impact of precession on monsoon characteristics from coupled ocean atmosphere experiments: changes in Indian monsoon and Indian ocean climatology, Marine Geology, 201, 23–34, 2003.

Braconnot, P., Marzin, C., Grégoire, L., Mosquet, E., and Marti, O.: Monsoon response to changes in Earth's orbital parameters: comparisons
310   between simulations of the Eemian and of the Holocene, Climate of the Past, 4, 281–294, 2008.

Cai, Y., Tan, L., Cheng, H., An, Z., Edwards, R. L., Kelly, M. J., Kong, X., and Wang, X.: The variation of summer monsoon precipitation in central China since the last deglaciation, Earth and Planetary Science Letters, 291, 21–31, 2010.

Carolin, S. A., Cobb, K. M., Adkins, J. F., Clark, B., Conroy, J. L., Lejau, S., Malang, J., and Tuen, A. A.: Varied response of western Pacific hydrology to climate forcings over the last glacial period, Science, 340, 1564–1566, 2013.

315 Carolin, S. A., Cobb, K. M., Lynch-Stieglitz, J., Moerman, J. W., Partin, J. W., Lejau, S., Malang, J., Clark, B., Tuen, A. A., and Adkins, J. F.: Northern Borneo stalagmite records reveal West Pacific hydroclimate across MIS 5 and 6, Earth and Planetary Science Letters, 439, 182–193, 2016.

Chen, F., Xu, Q., Chen, J., Birks, H. J. B., Liu, J., Zhang, S., Jin, L., An, C., Telford, R. J., Cao, X., et al.: East Asian summer monsoon precipitation variability since the last deglaciation, Scientific reports, 5, 1–11, 2015.

320 Cheng, H., Edwards, R. L., Broecker, W. S., Denton, G. H., Kong, X., Wang, Y., Zhang, R., and Wang, X.: Ice age terminations, science, 326, 248–252, 2009.

Cheng, H., Sinha, A., Cruz, F. W., Wang, X., Edwards, R. L., d'Horta, F. M., Ribas, C. C., Vuille, M., Stott, L. D., and Auler, A. S.: Climate change patterns in Amazonia and biodiversity, Nature communications, 4, 1411, 2013.

Cheng, H., Edwards, R. L., Sinha, A., Spötl, C., Yi, L., Chen, S., Kelly, M., Kathayat, G., Wang, X., Li, X., et al.: The Asian monsoon over
325   the past 640,000 years and ice age terminations, nature, 534, 640–646, 2016.

Cheng, H., Li, H., Sha, L., Sinha, A., Shi, Z., Yin, Q., Lu, Z., Zhao, D., Cai, Y., Hu, Y., et al.: Milankovitch theory and monsoon, The Innovation, 3, 2022.

Cheng, J., Wu, H., Liu, Z., Gu, P., Wang, J., Zhao, C., Li, Q., Chen, H., Lu, H., Hu, H., et al.: Vegetation feedback causes delayed ecosystem response to East Asian Summer Monsoon Rainfall during the Holocene, Nature Communications, 12, 1843, 2021.

330 Chiang, J. C. and Broccoli, A. J.: A role for orbital eccentricity in Earth's seasonal climate, Geoscience Letters, 10, 58, 2023.

17

Chiang, J. C. and Friedman, A. R.: Extratropical cooling, interhemispheric thermal gradients, and tropical climate change, Annual Review of Earth and Planetary Sciences, 40, 383–412, 2012.

Chiang, J. C., Atwood, A. R., Vimont, D. J., Nicknish, P. A., Roberts, W. H., Tabor, C. R., and Broccoli, A. J.: Two annual cycles of the Pacific cold tongue under orbital precession, Nature, 611, 295–300, 2022.

335 Clemens, S. C. and Prell, W. L.: The timing of orbital-scale Indian monsoon changes, Quaternary Science Reviews, 26, 275–278, 2007.

Clemens, S. C., Yamamoto, M., Thirumalai, K., Giosan, L., Richey, J. N., Nilsson-Kerr, K., Rosenthal, Y., Anand, P., and McGrath, S. M.: Remote and local drivers of Pleistocene South Asian summer monsoon precipitation: A test for future predictions, Science Advances, 7, eabg3848, 2021.

Clement, A. C., Hall, A., and Broccoli, A.: The importance of precessional signals in the tropical climate, Climate dynamics, 22, 327–341,
340   2004.

Cruz Jr, F. W., Burns, S. J., Karmann, I., Sharp, W. D., Vuille, M., Cardoso, A. O., Ferrari, J. A., Silva Dias, P. L., and Viana Jr, O.: Insolation-driven changes in atmospheric circulation over the past 116,000 years in subtropical Brazili, Nature, 434, 63–66, 2005.

Danilov, S., Sidorenko, D., Wang, Q., and Jung, T.: The finite-volume sea ice–ocean model (fesom2), Geoscientific Model Development, 10, 765–789, 2017.

345 DeMenocal, P. B., Tierney, J. E., et al.: Green Sahara: African humid periods paced by Earth's orbital changes, Nature Education Knowledge, 3, 12, 2012.

Donohoe, A., Dawson, E., McMurdie, L., Battisti, D. S., and Rhines, A.: Seasonal asymmetries in the lag between insolation and surface temperature, Journal of Climate, 33, 3921–3945, 2020.

Dykoski, C. A., Edwards, R. L., Cheng, H., Yuan, D., Cai, Y., Zhang, M., Lin, Y., Qing, J., An, Z., and Revenaugh, J.: A high-resolution,
350   absolute-dated Holocene and deglacial Asian monsoon record from Dongge Cave, China, Earth and Planetary Science Letters, 233, 71–86, 2005.

Erb, M. P., Jackson, C. S., and Broccoli, A. J.: Using single-forcing GCM simulations to reconstruct and interpret quaternary climate change, Journal of climate, 28, 9746–9767, 2015.

Gadgil, S.: The monsoon system: Land–sea breeze or the ITCZ?, Journal of Earth System Science, 127, 1–29, 2018.

355 Geen, R., Bordoni, S., Battisti, D. S., and Hui, K.: Monsoons, ITCZs, and the concept of the global monsoon, Reviews of Geophysics, 58, e2020RG000 700, 2020.

Giorgetta, M. A., Roeckner, E., Mauritsen, T., Bader, J., Crueger, T., Esch, M., Rast, S., Kornblueh, L., Schmidt, H., Kinne, S., et al.: The atmospheric general circulation model ECHAM6-model description, 2013.

Griffiths, M. L., Drysdale, R. N., Gagan, M., Zhao, J.-x., Ayliffe, L., Hellstrom, J. C., Hantoro, W., Frisia, S., Feng, Y.-x., Cartwright, I.,
360   et al.: Increasing Australian–Indonesian monsoon rainfall linked to early Holocene sea-level rise, Nature Geoscience, 2, 636–639, 2009.

He, F.: Simulating transient climate evolution of the last deglaciation with CCSM 3, vol. 72, University of Wisconsin–Madison, 2011.

Hunt, J., Lister, K., Nascimento, A., and Vasconcelos de Freitas, M.: The Ideal Climate Latitude: Orbit and Axial Precession Influence in Ancient Migration, Archaeology & Anthropology: Open Access, 4, 671–678, 2023.

Jalihal, C., Bosmans, J. H. C., Srinivasan, J., and Chakraborty, A.: The response of tropical precipitation to Earth's precession: the role of
365   energy fluxes and vertical stability, Climate of the Past, 15, 449–462, 2019.

Jian, Z., Wang, Y., Dang, H., Lea, D. W., Liu, Z., Jin, H., and Yin, Y.: Half-precessional cycle of thermocline temperature in the western equatorial Pacific and its bihemispheric dynamics, Proceedings of the National Academy of Sciences, 117, 7044–7051, 2020.

18

Joussaume, S. and Braconnot, P.: Sensitivity of paleoclimate simulation results to season definitions, Journal of Geophysical Research: Atmospheres, 102, 1943–1956, 1997.

370 Kelly, M. J., Edwards, R. L., Cheng, H., Yuan, D., Cai, Y., Zhang, M., Lin, Y., and An, Z.: High resolution characterization of the Asian Monsoon between 146,000 and 99,000 years BP from Dongge Cave, China and global correlation of events surrounding Termination II, Palaeogeography, Palaeoclimatology, Palaeoecology, 236, 20–38, 2006.

Kostadinov, T. and Gilb, R.: Earth Orbit v2. 1: a 3-D visualization and analysis model of Earth's orbit, Milankovitch cycles and insolation, Geoscientific Model Development, 7, 1051–1068, 2014.

375 Kuper, R. and Kropelin, S.: Climate-controlled Holocene occupation in the Sahara: motor of Africa's evolution, science, 313, 803–807, 2006.

Kutzbach, J., Liu, X., Liu, Z., and Chen, G.: Simulation of the evolutionary response of global summer monsoons to orbital forcing over the past 280,000 years, Climate Dynamics, 30, 567–579, 2008.

Kutzbach, J. E.: Monsoon climate of the early Holocene: climate experiment with the earth's orbital parameters for 9000 years ago, Science, 214, 59–61, 1981.

380 Kwiecien, O., Braun, T., Brunello, C. F., Faulkner, P., Hausmann, N., Helle, G., Hoggarth, J. A., Ionita, M., Jazwa, C. S., Kelmelis, S., et al.: What we talk about when we talk about seasonality–A transdisciplinary review, Earth-Science Reviews, 225, 103 843, 2022.

Lachniet, M. S.: Climatic and environmental controls on speleothem oxygen-isotope values, Quaternary Science Reviews, 28, 412–432, 2009.

Laskar, J.: The chaotic motion of the solar system: A numerical estimate of the size of the chaotic zones, Icarus, 88, 266–291, 1990.

385 Laskar, J., Joutel, F., and Boudin, F.: Orbital, precessional, and insolation quantities for the Earth from-20 Myr to+ 10 Myr, Astronomy and Astrophysics (ISSN 0004-6361), vol. 270, no. 1-2, p. 522-533., 270, 522–533, 1993.

Li, X., Zhou, Y., Han, Z., Yuan, X., Yi, S., Zeng, Y., Qin, L., Lu, M., and Lu, H.: Loess deposits in the low latitudes of East Asia reveal the 20-kyr precipitation cycle, Nature Communications, 15, 1023, 2024.

Lisiecki, L. E. and Raymo, M. E.: A Pliocene-Pleistocene stack of 57 globally distributed benthic δ18O records, Paleoceanography, 20, 2005.

390 Liu, J., Chen, J., Zhang, X., Li, Y., Rao, Z., and Chen, F.: Holocene East Asian summer monsoon records in northern China and their inconsistency with Chinese stalagmite δ18O records, Earth-Science Reviews, 148, 194–208, 2015.

Liu, X., Xie, X., Guo, Z., Yin, Z.-Y., and Chen, G.: Model-based orbital-scale precipitation δ18O variations and distinct mechanisms in Asian monsoon and arid regions, National Science Review, 9, nwac182, 2022.

Liu, Z., Otto-Bliesner, B., He, F., Brady, E., Tomas, R., Clark, P., Carlson, A., Lynch-Stieglitz, J., Curry, W., Brook, E., et al.: Transient
395 simulation of last deglaciation with a new mechanism for Bølling-Allerød warming, science, 325, 310–314, 2009.

Lougheed, B. C.: Orbital, the Box-An interactive educational tool for in-depth understanding of astronomical climate forcing., 2021.

Lyu, A., Yin, Q., Crucifix, M., and Sun, Y.: Diverse regional sensitivity of summer precipitation in East Asia to ice volume, CO2 and astronomical forcing, Geophysical Research Letters, 48, e2020GL092 005, 2021.

Milankovitch, M.: Canon of Insolation and the Ice Age Problem (in German), Königlich Serbische Akademie, 1941.

400 Neelin, J. D. and Held, I. M.: Modeling tropical convergence based on the moist static energy budget, Monthly Weather Review, 115, 3–12, 1987.

Ran, M. and Feng, Z.: Holocene moisture variations across China and driving mechanisms: A synthesis of climatic records, Quaternary International, 313, 179–193, 2013.

Schneider, T., Bischoff, T., and Haug, G. H.: Migrations and dynamics of the intertropical convergence zone, Nature, 513, 45–53, 2014.

405 Shanahan, T. M., McKay, N. P., Hughen, K. A., Overpeck, J. T., Otto-Bliesner, B., Heil, C. W., King, J., Scholz, C. A., and Peck, J.: The time-transgressive termination of the African Humid Period, Nature Geoscience, 8, 140–144, 2015.

Shi, X. and Lohmann, G.: Simulated response of the mid-Holocene Atlantic meridional overturning circulation in ECHAM6-FESOM/MPIOM, Journal of Geophysical Research: Oceans, 121, 6444–6469, 2016.

Shi, X., Werner, M., Krug, C., Brierley, C. M., Zhao, A., Igbinosa, E., Braconnot, P., Brady, E., Cao, J., d'Agostino, R., et al.: Calendar effects
410 on surface air temperature and precipitation based on model-ensemble equilibrium and transient simulations from PMIP4 and PACMEDY, Climate of the Past, 18, 1047–1070, 2022.

Short, D. A. and Mengel, J. G.: Tropical climatic phase lags and Earth's precession cycle, Nature, 323, 48–50, 1986.

Sidorenko, D., Rackow, T., Jung, T., Semmler, T., Barbi, D., Danilov, S., Dethloff, K., Dorn, W., Fieg, K., Gößling, H. F., et al.: Towards multi-resolution global climate modeling with ECHAM6–FESOM. Part I: model formulation and mean climate, Climate Dynamics, 44,
415 757–780, 2015.

Sidorenko, D., Goessling, H., Koldunov, N., Scholz, P., Danilov, S., Barbi, D., Cabos, W., Gurses, O., Harig, S., Hinrichs, C., et al.: Evaluation of FESOM2. 0 coupled to ECHAM6. 3: preindustrial and HighResMIP simulations, Journal of Advances in Modeling Earth Systems, 11, 3794–3815, 2019.

Sun, Y., Chen, J., Clemens, S. C., Liu, Q., Ji, J., and Tada, R.: East Asian monsoon variability over the last seven glacial cycles recorded by
420 a loess sequence from the northwestern Chinese Loess Plateau, Geochemistry, Geophysics, Geosystems, 7, 2006.

Thamban, M., Kawahata, H., and Rao, V. P.: Indian summer monsoon variability during the Holocene as recorded in sediments of the Arabian Sea: timing and implications, Journal of oceanography, 63, 1009–1020, 2007.

Trauth, M. and Strecker, M.: Late Pleistocene lake-level fluctuations in the Naivasha Basin, Kenya, in: Limnology, Climatology and Paleo-climatology of the East African Lakes, pp. 549–557, Routledge, 1996.

425 Trauth, M. H., Deino, A. L., Bergner, A. G., and Strecker, M. R.: East African climate change and orbital forcing during the last 175 kyr BP, Earth and Planetary Science Letters, 206, 297–313, 2003.

Verschuren, D., Sinninghe Damsté, J. S., Moernaut, J., Kristen, I., Blaauw, M., Fagot, M., and Haug, G. H.: Half-precessional dynamics of monsoon rainfall near the East African Equator, Nature, 462, 637–641, 2009.

Wallace, J. M. and Hobbs, P. V.: Atmospheric science: an introductory survey, vol. 92, Elsevier, 2006.

430 Wang, B. and Ding, Q.: Global monsoon: Dominant mode of annual variation in the tropics, Dynamics of Atmospheres and Oceans, 44, 165–183, 2008.

Wang, P., Wang, B., Cheng, H., Fasullo, J., Guo, Z., Kiefer, T., and Liu, Z.: The global monsoon across timescales: coherent variability of regional monsoons, Climate of the Past, 10, 2007–2052, 2014a.

Wang, P. X., Wang, B., Cheng, H., Fasullo, J., Guo, Z., Kiefer, T., and Liu, Z.: The global monsoon across time scales: Mechanisms and
435 outstanding issues, Earth-Science Reviews, 174, 84–121, 2017.

Wang, Q., Danilov, S., Sidorenko, D., Timmermann, R., Wekerle, C., Wang, X., Jung, T., and Schröter, J.: he Finite Element Sea Ice-Ocean Model (FESOM) v. 1.4: formulation of an ocean general circulation model, Geoscientific Model Development, 7, 663–693, 2014b.

Wang, X., Auler, A. S., Edwards, R. L., Cheng, H., Cristalli, P. S., Smart, P. L., Richards, D. A., and Shen, C.-C.: Wet periods in northeastern Brazil over the past 210 kyr linked to distant climate anomalies, Nature, 432, 740–743, 2004.

440 Wang, X., Auler, A. S., Edwards, R., Cheng, H., Ito, E., Wang, Y., Kong, X., and Solheid, M.: Millennial-scale precipitation changes in southern Brazil over the past 90,000 years, Geophysical Research Letters, 34, 2007.

Wang, Y., Cheng, H., Edwards, R. L., Kong, X., Shao, X., Chen, S., Wu, J., Jiang, X., Wang, X., and An, Z.: Millennial-and orbital-scale changes in the East Asian monsoon over the past 224,000 years, Nature, 451, 1090–1093, 2008.

Wang, Y.-J., Cheng, H., Edwards, R. L., An, Z., Wu, J., Shen, C.-C., and Dorale, J. A.: A high-resolution absolute-dated late Pleistocene

445   monsoon record from Hulu Cave, China, Science, 294, 2345–2348, 2001.

Weber, S. and Tuenter, E.: The impact of varying ice sheets and greenhouse gases on the intensity and timing of boreal summer monsoons, Quaternary Science Reviews, 30, 469–479, 2011.

Wu, C.-H., Lee, S.-Y., Chiang, J. C., and Tsai, P.-C.: Role of precession on the transition seasons of the Asian monsoon, npj Climate and Atmospheric Science, 6, 95, 2023.

450   Yuan, S., Chiang, H.-W., Liu, G., Bijaksana, S., He, S., Jiang, X., Imran, A. M., Wicaksono, S. A., and Wang, X.: The strength, position, and width changes of the intertropical convergence zone since the Last Glacial Maximum, Proceedings of the National Academy of Sciences, 120, e2217064 120, 2023.

Zhao, Y., Braconnot, P., Marti, O., Harrison, S., Hewitt, C., Kitoh, A., Liu, Z., Mikolajewicz, U., Otto-Bliesner, B., and Weber, S.: A multi-model analysis of the role of the ocean on the African and Indian monsoon during the mid-Holocene, Climate Dynamics, 25, 777–800,

455   2005.

Zhou, X., Zhan, T., Tu, L., Smol, J. P., Jiang, S., Liu, X., Xu, C., and Guo, Z.: Monthly insolation linked to the time-transgressive nature of the Holocene East Asian monsoon precipitation maximum, Geology, 50, 331–335, 2022.